NSRRC-J04640(2015)

Macromolecules

Article

pubs.acs.org/Macromolecules

Phase Behavior and Structure of Supramolecules Formed by Poly(4-vinylpyridine) and Fanlike Benzoic Acid Derivative with Long Hydrophobic Tails

Tzu-Yu Lai,[†] Chih-Yang Cheng,[†] Wan-Yin Cheng,[‡] Kwang-Ming Lee,*[,‡] and Shih-Huang Tung*[,†]

[†]Institute of Polymer Science and Engineering, National Taiwan University, Taipei 10617, Taiwan

[‡]Department of Chemistry, National Kaohsiung Normal University, Kaohsiung 82444, Taiwan

Supporting Information

ABSTRACT: We investigated the self-assembly behaviors of supramolecules formed by poly(4-vinylpyridine) (P4VP) and a fanlike small molecule, 3,4,5-tris(hexadecyloxy)benzoic acid (THBA), via hydrogen bonding interactions. Different from other commonly studied small molecules, THBA bears three particularly long hydrophobic tails and tends to form stable crystals by itself, which gives rise to unusual phase behaviors and structures. We used FTIR to investigate the degree of complexation and find that it is not monotonically increased to a plateau with increasing THBA but reaches a maximum and then decreased. This is attributed to the crystallization of excess THBA that induces a debonding of the originally associated THBA. The crystallization-induced dissociation and macrophase separation are further evidenced by DSC and X-ray scattering analyses. Below the order−disorder transition temperature, a coexistence of lamellae and hexagonally packed cylinders is found in melted P4VP(THBA) supramolecules. After the associated THBA crystallizes, the complexes exclusively form hexagonally packed cylinders due to the bulky tails of THBA, in the absence of the lamellar structure generally seen in other polymer-based supramolecules.

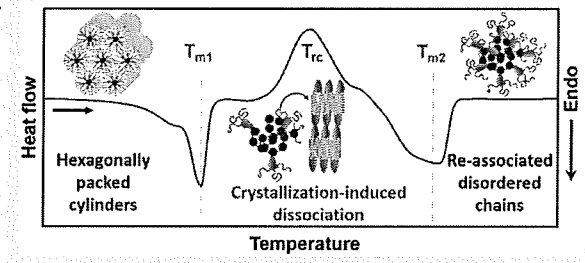

1. INTRODUCTION

By incorporating small molecules into polymer, the resulting supramolecules may possess various self-organized morphologies and versatile properties, which has received much attention recently.[1−7] This complexation is achieved by noncovalent interactions, including electrostatic interactions, hydrogen bonding, and metal−ligand coordination bonding, between polymer and small molecules.[8−11] By tuning the content of small molecules that generally act as side groups to alter the conformation and architecture of polymer chains, the complexation triggers an evolution of microphase-separated structure. Furthermore, small molecules have been introduced into block copolymers, and even more diversified hierarchical structures have been created.[1,2,5,12−16] Since the physical complexation can be easily achieved, the properties of polymers become highly tunable through incorporating appropriate small molecules, such as stiffening of flexible backbones or plasticizing of polymers to increase solubility and fusibility.[17,18] More importantly, a variety of functionalities can be imparted into polymers by this strategy, such as optical and electrical responses.[6,19,20] The study of polymer-based supramolecules thus paves a way to obtain desired properties and designable morphologies by simply mixing small molecules and polymers without the complicated synthesis of analogous polymeric architectures.[21,22]

The self-assembly behaviors of polymer-based supramolecules have been extensively studied, especially for those composed of poly(4-vinylpyridine) (P4VP) whose pyridine group acts as a proton acceptor.[1,10,14,16,23−29] It has been shown that the intermolecular attraction forces and the incompatibility between polymer and small molecules dominate the phase behavior and structure within supramolecules.[30,31] The formation of mesomorphic structures requires sufficiently strong secondary bonds that hold small molecules and polymer together, and enthalpically, the capability of forming such bonds is determined by the net effect from the competition between polymer−small molecule interactions and the interactions in the same molecules.[30] In the presence of a strong association, the incompatibility between polymer and the hydrophobic alkyl chains on small molecules may cause a microphase separation that form an ordered mesomorphic structure below order−disorder transition (ODT) temperature. The incompatibility can be strengthened by increasing alkyl chain length or by adding charges to polymer backbone, which in turn causes ODT temperature to increase.[10,25,32] The common feature of the supramolecules formed by polymers

Received: October 31, 2014
Revised: January 13, 2015
Published: January 28, 2015

ACS Publications © 2015 American Chemical Society

DOI: 10.1021/ma5022192
Macromolecules 2015, 48, 717−724

and linear small molecules is that the resulting comblike chains generally self-assemble into lamellar mesophases.

Recently, wedge-shaped or fanlike small molecules have been designed to associate with homopolymers or block copolymers to form supramolecules. In addition to lamellar mesophase, these supramolecules are capable of forming ordered liquid-crystalline structures with hexagonal columnar phase.[4,7,28,33−35] This type of small molecule generally bears sulfonic acid,[33] benzoic acid,[7,28] or phenol[34] that are able to associate with polymers and contains three alkyl tails that provide a large hydrophobic body. In the reported cases where the length of the tails is up to 14 carbons, when the fanlike small molecules are grafted onto polymer chains at a low degree of complexation, the self-assembled structure of the supramolecules remains lamellar. Above a critical point, the polymer chains become fully jacketed by the bulky tails and thus form polymer brushes with well-defined cylindrical structure that prefer to pack hexagonally. A transition from lamellar to hexagonally packed cylinder (HPC) mesophase can therefore be observed as the amount of associated small molecules increases. Because of the large tail volume that generates severer steric repulsion, the saturated degree of complexation for fanlike molecules is generally lower than that of linear counterparts.

In this paper, we investigated the supramolecular assemblies composed of fanlike benzoic acid derivative, 3,4,5-tris-(hexadecyloxy)benzoic acid (THBA), hydrogen-bonded with P4VP homopolymers of two different molecular weights (Figure 1). The 16-carbon tails of THBA are longer than those of other fanlike molecules reported previously.[4,7,28,33−35] The tail length may affect the self-assembly of supramolecules in two aspects. First, longer tails tend to form more stable crystals due to a smaller change of entropy upon fusion. The self-crystallization of small molecules may compete with the association of small molecules and polymer, thus reducing the net attractive interactions. Our experiences show that 16 carbons are the upper limit of tail length for such fanlike benzoic acid derivatives to efficiently associate with P4VP. Second, longer tails aggravate steric repulsion, which may alter the architecture of supramolecular chains as well as the resulting self-assembled structures. To obtain a clearer picture of the interplay between polymer and fanlike small molecules, we used FTIR to quantify the degree of complexation and to demonstrate how the self-crystallization of small molecules influences the complexation in polymer-based supramolecules. X-ray scattering, differential scanning calorimetry (DSC), and polarized optical microscopy (POM) were utilized to elucidate the dependence of phase behaviors on composition and temperature. We find that the marginal tail length of THBA brings about more diversified phase behaviors than others do, as will be shown in this paper.

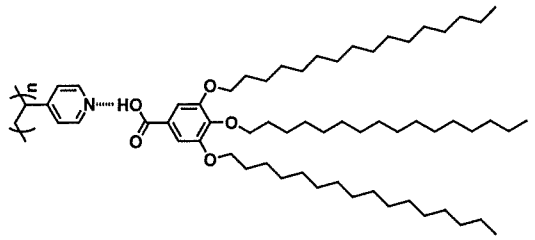

Figure 1. Chemical structures of P4VP and THBA. The carboxylic group on THBA associates with the pyridine group on P4VP via hydrogen bonding.

2. EXPERIMENTAL SECTION

2.1. Materials. $P4VP_{1.7k}$ (M_n = 1760 g/mol, PDI = 1.19) and $P4VP_{15k}$ (M_n = 15 000 g/mol, PDI = 1.25) were purchased from Polymer Source. P4VP was dried overnight in vacuum at 100 °C before used. Chloroform (≥99.8%) was purchased from Avantor Performance Materials and used without further purification. The synthesis procedure[36] and the characterization of 3,4,5-tris-(hexadecyloxy)benzoic acid (THBA) are detailed in the Supporting Information.

2.2. Sample Preparation. The desired amount of P4VP and small molecules were separately dissolved in chloroform to form ~3 wt % solutions. The polymer solutions were then sequentially added to the small molecule solutions, followed by stirring for days. Subsequently, the supramolecular samples were collected by a slow evaporation of solvent in Teflon beakers. The samples were then annealed under a nitrogen atmosphere at 85 °C for 2 days. After thermal annealing, the samples were slowly cooled to room temperature. The supramolecular samples are denoted as $P4VP_n(THBA)_x$, where n is the molecular weight of P4VP and x is the molar ratio of THBA to the repeat unit of P4VP.

2.3. Fourier Transform Infrared Spectroscopy (FTIR). The mixed solutions were cast onto KBr pellets and the samples were dried at room temperature. The samples were annealed at 85 °C and then slowly cooled down to room temperature under nitrogen. FTIR spectra were recorded in the transmission mode by a PerkinElmer Spectrum 100 Model FTIR spectrometer from an accumulation of 16 scans at 1 cm^{-1} resolution. For *in situ* FTIR measurements, the samples were heated from room temperature to 100 °C. The heating rate was ~1 °C/min, and each spectrum was collected at 2 min after reaching the target temperature.

2.4. X-ray Scattering. Transmission-mode small-angle and wide-angle X-ray scattering (SAXS and WAXS) were carried out on beamline B23A1 in the National Synchrotron Radiation Research Center (NSRRC), Taiwan, and a wavelength λ of 0.827 Å was used.[37] The 1-D scattering intensity profiles were obtained by circularly averaging the 2-D patterns and reported as the plots of scattering intensity I versus the scattering vector q, where $q = (4\pi/\lambda)\sin(\theta/2)$ and θ is the scattering angle. The scattering angle was calibrated using silver behenate as the standard.

2.5. Differential Scanning Calorimetry (DSC). DSC measurements were performed on a TA Instruments DSC Q200 under a nitrogen atmosphere. Indium was used as the standard for temperature calibration. Samples were encapsulated in sealed aluminum pans, and the weight was ~3 mg. The thermal treatments and heating rates for the measurements were dependent on the experimental demands and will be noted in the text.

2.6. Polarized Optical Microscopy (POM). POM instrument was performed on an Olympus BX51 M microscope with crossed polarizers in reflection mode. Samples sandwiched between a glass slide and a cover glass were first melted at 90 °C and then cooled at a rate of 1 °C/min for *in situ* observation. The thermal treatments were conducted on a Linkam THMS600 heating stage with a Linkam CI94 temperature controller.

3. RESULTS AND DISCUSSION

3.1. Complexation between P4VP and THBA. We first discuss the degree of complexation between the carboxylic group of THBA and the pyridine of P4VP via hydrogen bonding. Figure 2 shows the FTIR spectra of supramolecular assemblies $P4VP_{15k}(THBA)_x$ with different molar ratio x of THBA:4VP. The characteristic bands at 1597 and 993 cm^{-1} correspond to the stretching mode of the free pyridine ring on pristine P4VP.[31] Because of the formation of hydrogen bonds with THBA, the 1597 cm^{-1} band shifts to 1607 cm^{-1} and the 993 cm^{-1} band shifts to 1014 cm^{-1}. The intensities of the

DOI: 10.1021/ma5022192
Macromolecules 2015, 48, 717−724

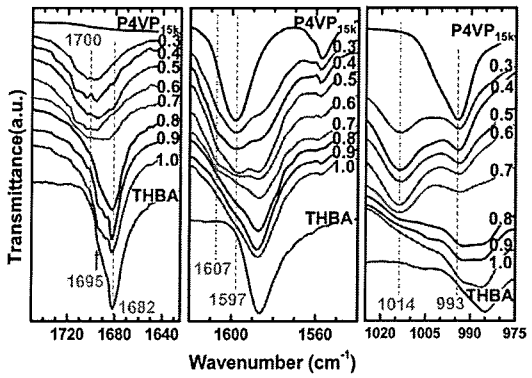

Figure 2. FTIR spectra of THBA, $P4VP_{15k}$ and $P4VP_{15k}(THBA)_x$ samples.

hydrogen-bonded bands (1607 and 1014 cm^{-1}) are found to increase with increasing x until 0.6. At $x > 0.8$, the absorptions of the hydrogen-bonded bands unusually diminish with increasing x. This suggests a maximum complexation between THBA molecules and the pyridine rings. A similar result is found for C=O bands of THBA. Pure THBA with C=O groups involving in strong intermolecular hydrogen bonding shows the absorption bands at 1682 and 1695 cm^{-1}. At $x < 0.7$, the bands shift to ~1700 cm^{-1} because the C=O groups are free from hydrogen bonding in P4VP(THBA) complexes (Figure 1).[24,38] The 1700 cm^{-1} bands sharply weaken and the pure THBA bands become dominant at $x \geq 0.8$, apparently due to a disproportionate increase of excess THBA that are not associated with P4VP. We have also observed that at high x ($\geq$0.8) the samples become cloudy, indicating that THBA macrophase separates out from P4VP and self-crystallize.[23,24] $P4VP_{1.7k}(THBA)_x$ samples show similar trend (Figure S1 in the Supporting Information), but with the most pronounced complexation-caused band shifts at a lower x, ~0.5, compared to that of $P4VP_{15k}(THBA)_x$.

We further quantify the degree of complexation by deconvolution of the FTIR spectra in the range of 1545–1620 cm^{-1}. The spectra here can be separated into four absorption bands as shown in Figure S2 of the Supporting Information.[28] In addition to the 1597 and 1607 cm^{-1} bands of the free and hydrogen-bonded pyridine ring, the bands at 1587 and 1557 cm^{-1} are characteristic of THBA benzene ring and P4VP pyridine ring, respectively, which are insensitive to complexation. The spectra are deconvoluted by Gaussian amplitude function with the PeakFit software. The degree of complexation (f_{HB}) can be estimated by the equation[1,28,39]

$$f_{HB} = \frac{A_{1607}}{A_{1607} + \frac{\alpha_{1597}}{\alpha_{1607}} A_{1597}} \quad (1)$$

where A and α are the peak area and the absorption coefficient at 1607 and 1597 cm^{-1}. Here we use the insensitive band at 1557 cm^{-1} as a reference. Since the area of the band (A_{1557}) over the total area of all the three pyridine bands ($A_{1557} + A_{1597} + A_{1607}$) for each sample is approximately a constant (~0.16), $\alpha_{1597}/\alpha_{1607}$ can be assumed to be 1.[1,39,40] The equation can thus be simplified to

$$f_{HB} = \frac{A_{1607}}{A_{1607} + A_{1597}} \quad (2)$$

The estimated degree of complexation is illustrated in Figure 3. The maximum complexation is around 60% and 46% for

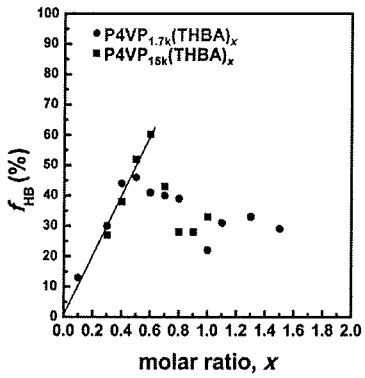

Figure 3. Degree of complexation (f_{HB}) as a function of molar ratio x for $P4VP_{15k}(THBA)_x$ and $P4VP_{1.7k}(THBA)_x$.

$P4VP_{15k}(THBA)_{0.6}$ and $P4VP_{1.7k}(THBA)_{0.5}$, respectively. Above the maximum x, the addition of more THBA molecules causes the value of f_{HB} to decrease, which is different from the effect of the fanlike small molecule with dodecyl tails reported by Wang et al.[28] In their study, the value of f_{HB} remains constant at a saturated complexation level when x is above a critical value. Such a difference is attributed to the higher tendency of THBA to crystallize due to its long hexadecyl tails. The crystallization of the excess, free THBA molecules under cooling process may initiate a dissociation of THBA from P4VP that lowers the degree of complexation.[29] From the standpoint of thermodynamics, the dissociation requires heat absorption to overcome the THBA–P4VP hydrogen bonds and also a demixing process causes the mixing entropy to decrease, both of which increase the free energy against dissociation. However, the release of THBA intermolecular interaction energy from the self-crystallization of THBA is favorable for dissociation. At high x values, the latter dominates over the former so that the dissociation occurs.

3.2. Structure of $P4VP(THBA)_x$. In this section, we focus on the structural characterization of the bulk samples after annealing and slow cooling in oven. Figure 4 shows the SAXS and WAXS profiles of pure THBA and $P4VP_{15k}(THBA)_x$ samples. Pure THBA crystals reveal diffraction peaks at q = 0.129, 0.258, and 0.387 $Å^{-1}$ in SAXS data (Figure 4a), a perfect 1:2:3 ratio that infers a lamellar structure with a d-spacing of 4.9 nm. Note that the second-order peak is barely seen. This is ascribed to the equal thickness of the two alternating layers with which the even-order maxima of the structure factor are exactly at the same q values where the form factor of the layers is at the minimums.[41] The total scattering intensities of the even-order peaks are thus greatly reduced. The lamellar structure in THBA crystals is illustrated in Figure S3 of the Supporting Information. The benzoic acid groups with intermolecular hydrogen bonds form one alternating layer and the fully strengthened, interdigitated alkyl tails form the other. The close packing of the benzoic acids and alkyl tails give rise to the multiple diffraction peaks around 1.5 $Å^{-1}$ in WAXS data (Figure 4b).

For $P4VP_{15k}(THBA)_x$ samples at $x \leq 0.3$, only one broad hump between 0.1 and 0.15 $Å^{-1}$ is observed in SAXS profiles. The hump represents the correlation length between the

DOI: 10.1021/ma5022192
Macromolecules 2015, 48, 717–724

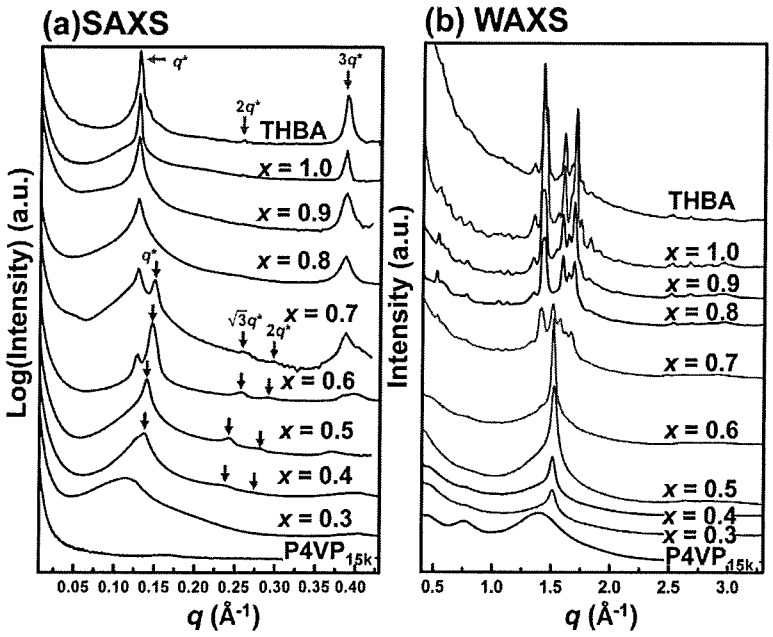

Figure 4. (a) SAXS and (b) WAXS profiles of THBA and $P4VP_{15k}(THBA)_x$ samples at room temperature.

disordered supramolecular chains. The lack of sharp peaks implies the amount of THBA molecules is insufficient to create an ordered structure. When x reaches 0.4, the characteristic peaks of hexagonally packed cylinders (HPC) in a $1:\sqrt{3}:2$ ratio appear. With enough THBA molecules grafted onto P4VP chains, the supramolecules form an ordered HPC structure of a d-spacing ~4.5 nm estimated from the first-order peak. The peaks become even sharper at $x = 0.5$ and slightly shift to higher q until $x = 0.7$, indicating a decrease of d-spacing. This can be rationally explained by the fact that the attachment of more THBA molecules onto P4VP causes a more stretched P4VP backbone, and thus the center-to-center distance between P4VP(THBA) cylinder-like chains is reduced.[5,28] In the WAXS profile, once the HPC structure is formed, the packing of the associated THBA molecules produces a sharp peak at 1.52 $Å^{-1}$ (d-spacing ~4.1 Å). At $x = 0.6$, in addition to the HPC characteristic peaks, the peak of pure THBA crystals shows up in the SAXS profile. This peak dominates over the HPC characteristic peaks and remains at a constant q for $x \geq 0.7$. Meanwhile, the group of peaks attributed to pure THBA crystals appear around 1.50 $Å^{-1}$ in the WAXS profiles. In other words, there is a significant amount of excess THBA molecules unable to associate with P4VP at $x \geq 0.7$. When x is above 0.8, in both SAXS and WAXS profiles, only the peaks of pure THBA crystals can be seen, implying that a macrophase separation occurs; that is, the original bonded THBA molecules are detached to form crystal phases, and the HPC structure nearly disappears.

The X-ray scattering data of $P4VP_{1.7k}(THBA)_x$ samples are shown in Figure S4 of the Supporting Information. The trend is similar, with only slightly different x range of morphology transition. In $P4VP_{1.7k}(THBA)_x$ series, the HPC structures are formed in a narrower x range, between 0.5 and 0.6, which may be due to the lower aspect ratio of shorter P4VP chains that are less capable of arranging into ordered structures. The peak at 1.52 $Å^{-1}$ in WAXS profiles from the packing of associated THBA molecules is the same as that of $P4VP_{15k}(THBA)_x$ samples. At $x = 0.6$, the diffraction peaks from pure THBA crystals arise in both SAXS and WAXS profiles, and above 0.7, these diffraction peaks become completely dominant. In both $P4VP_{15k}(THBA)_x$ and $P4VP_{1.7k}(THBA)_x$ systems, the results of the X-ray scattering measurements are consistent with the FTIR analysis (Figure 2 and Figure S1): as the molar ratio x exceeds the limit of complexation, the bonded THBA molecules are susceptible to dissociating from P4VP when THBA self-crystallizes. Note that the commonly occurring lamellar structures of polymer-based comblike supramolecules are not observed here even though pure THBA crystallizes into lamellar structure.[28,34,35] Small molecules with the long, bulky alkyl tails may wrap around the polymer backbone and lead to the formation of extended brushlike supramolecules in cylindrical shape due to the strong steric repulsion between the small molecules.[1,30,31,42]

3.3. Thermal Behaviors. DSC was unitized to study the phase transition of $P4VP(THBA)_x$ supramolecules which were prepared in the same manner as those for X-ray scattering experiments. Figure 5 shows the DSC data of $P4VP_{15k}(THBA)_x$ at a heating rate of 10 °C/min. The melting point of pure THBA is 82 °C. At $x \leq 0.6$, the major endothermic peak is around 45 °C, which is far below that of pure THBA and should be rationally assigned to the melting of the crystals formed by associated THBA. When x is above 0.4, another melting peak between 70 and 80 °C close to that of pure THBA can be seen. This comes from the crystals of free THBA molecules in the presence of impurity (P4VP in this case). Both the melting temperature and the melting latent heat increase with x. Above 0.7, the melting heat of associated THBA sharply decreases while that of free THBA become much more pronounced, in agreement with the FTIR and X-ray scattering results that $x = 0.6$ is approximately the upper limit of complexation for $P4VP_{15k}(THBA)_x$. $P4VP_{1.7k}(THBA)_x$ series show a very similar trend as displayed in Figure S5 of the Supporting Information. The melting peak of free THBA

DOI: 10.1021/ma5022192
Macromolecules 2015, 48, 717−724

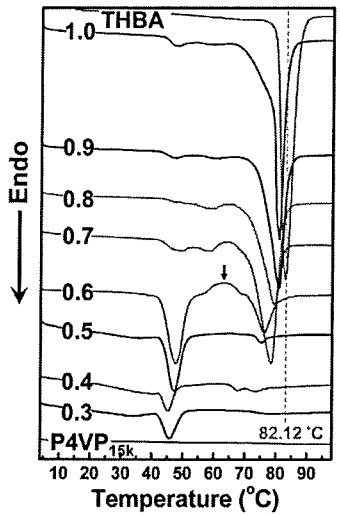

Figure 5. DSC profiles of annealed $P4VP_{15k}(THBA)_x$ samples at a heating rate of 10 °C/min. The arrow indicates the recrystallization of dissociated THBA for $x = 0.6$.

crystals dominates at $x = 0.6$, implying the maximum complexation is around 0.5.

It is worth noting that a broad exothermic peak appears at ~64 °C for $x = 0.6$ sample as indicated by the arrow in Figure 5, which is apparently contributed from the recrystallization of free THBA molecules. The crystals that form at this temperature then melt at ~76 °C, and the melting heat is nearly the same as the recrystallization heat, ~18 J/g. It has been shown that almost all the THBA molecules associate with P4VP in this sample, and also, since the cooling rate in oven is very slow, both associated and free (if any) THBA molecules should completely crystallize during cooling process. The recrystallization is thus not from the uncrystallized free THBA, but from the dissociated THBA molecules that are originally hydrogen-bonded with P4VP. After the melting of the hydrogen-bonded THBA crystals at ~48 °C, THBA molecules incline to detach from P4VP and form crystals at ~64 °C. This phenomenon again reveals that the high tendency of free THBA molecules to crystallize may force the associated THBA molecules to dissociate from P4VP.

The recrystallization-induced dissociation can also be observed at a slow heating rate, 1 °C/min, in $P4VP_{1.7k}(THBA)_{0.5}$ sample as shown in Figure 6. At such a slow heating rate, a pronounced recrystallization of dissociated THBA molecules occurs at ~56 °C followed by a melting at 71 °C. The recrystallization and melting heats are nearly the same, ~51 J/g. Note that this recrystallization is not clearly seen at a heating rate of 10 °C/min shown in Figure S5 because the time frame is too short for a significant recrystallization to take place. We conducted *in situ* FTIR on heating to investigate the dependence of P4VP–THBA complexation on temperature, and the data are shown in Figure 7. The bands of hydrogen-bonded pyridine at 1607 and 1014 cm^{-1} and the C=O bands of associated THBA at 1700 cm^{-1} are much weakened between 55 and 70 °C, exactly in the temperature range where the recrystallization and melting occur. The recrystallization-induced dissociation is thus evidenced. It is interesting that above 75 °C the characteristic bands from the complexation of P4VP and THBA become pronounced again, implying that

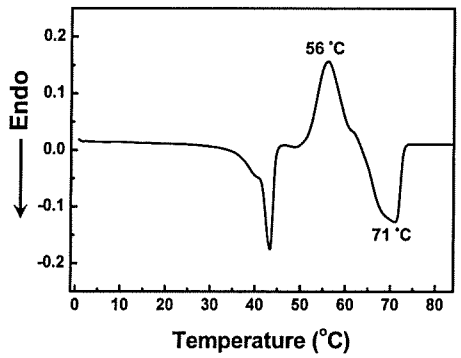

Figure 6. DSC profile of $P4VP_{1.7k}(THBA)_{0.5}$ at a heating rate of 1 °C/min after the sample is slowly cooled down from melt.

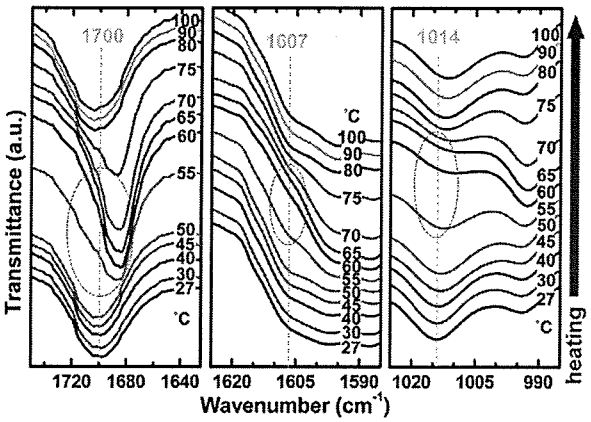

Figure 7. *In situ* FTIR spectra of $P4VP_{1.7k}(THBA)_{0.5}$ on heating. The temperature ranges of recrystallization and melting are circled by the dashed lines.

after free THBA crystals melt, THBA molecules tend to attach back to P4VP even at high temperature. The DSC heating profile of $P4VP_{15k}(THBA)_{0.5}$ at a slow heating rate of 1 °C/min is shown in Figure S6, and a similar recrystallization can be found. The *in situ* SAXS and WAXS data of the sample on heating are shown in Figure S7 of the Supporting Information where the appearance of the diffraction peaks from free THBA crystals between 54 and 71 °C confirms the recrystallization is from dissociated THBA.

3.4. Temperature-Dependent Phase Transition. In this section, the phase transition in the cooling process is elucidated by DSC and scattering techniques. Figure 8 shows the DSC curves of $P4VP_{15k}(THBA)_x$ at a slow cooling rate of 1 °C/min. For the samples at $0.3 \leq x \leq 0.8$, a small exothermic peak appears between 65 and 70 °C (red arrows), and two adjacent exothermic peaks are found between 25 and 40 °C (blue and green arrows) during cooling process. To identify these transitions, *in situ* SAXS and WAXS were used to probe the temperature-dependent structures of $P4VP_{15k}(THBA)_{0.5}$ as shown in Figure 9. In Figure 9a, after the sample is cooled to ~67 °C, the diffraction peak at $q = 0.153$ $Å^{-1}$ becomes very sharp, and the higher-order peaks are in order of $1:\sqrt{3}:2$, indicating the exothermic peak between 65 and 70 °C shown in Figure 8 is the order–disorder transition (ODT) temperature.[43] Below 30 °C, the appearance of sharp diffraction peaks at $q = 1.51$ $Å^{-1}$ in WAXS profiles (Figure 9b) suggests that the

DOI: 10.1021/ma5022192
Macromolecules 2015, 48, 717–724

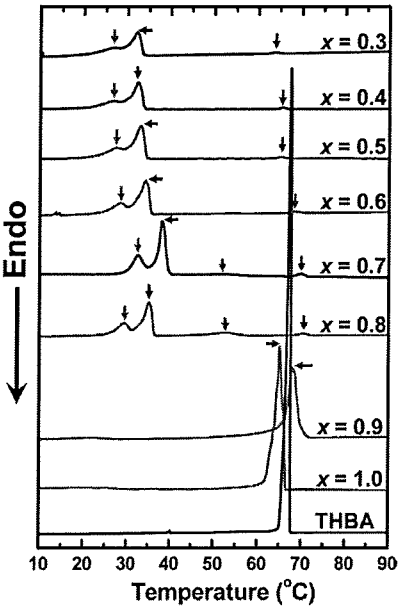

Figure 8. DSC profiles of $P4VP_{15k}(THBA)_x$ at a cooling rate 1 °C/min. The peaks of the self-crystallization of free THBA molecules, the order–disorder transition, the crystallization of associated THBA, and the crystal reorganization are marked with the purple, red, blue, and green arrows, respectively.

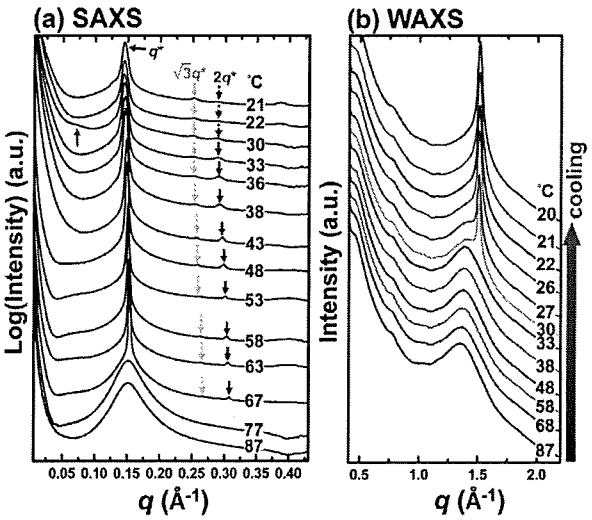

Figure 9. *In situ* (a) SAXS and (b) WAXS profiles of $P4VP_{15k}(THBA)_{0.5}$ at a cooling rate ~1 °C/min. The dashed arrows for $\sqrt{3}q^*$ peaks indicate the intensities of the peaks are weaker than those of the corresponding $2q^*$ peaks. The green arrow labels the diffraction from the cocrystals of associated and free THBA.

exothermic peaks between 25 and 40 °C in the DSC curve correspond to the crystallization of associated THBA. At x = 0.7 and 0.8 where excess THBA is present, in addition to the above-mentioned exothermic peaks, the crystallization of excess THBA molecules causes an extra broad exothermic hump at ~50 °C as indicated by the purple arrows (Figure 8). At $x \geq$ 0.9, because of the high tendency of free excess THBA molecules to crystallize, only the exothermic peak close to the crystallization peak of pure THBA can be seen.

Taking a careful look into the SAXS profiles of $P4VP_{15k}(THBA)_{0.5}$ in Figure 9, it can be found that around the ODT temperature (63 and 67 °C) the $\sqrt{3}q^*$ peak is nearly invisible, and a relatively pronounced 1:2 ratio indicates a lamellar structure dominates at this temperature range. The intensity of $\sqrt{3}q^*$ peak gradually increases on cooling but is still weaker than that of $2q^*$ peak even down to 33 °C. This suggests a coexistence of lamellar and HPC structures with nearly the same largest d-spacing between ODT and 33 °C, and the lamellae are slowly transformed into cylinders. Below 30 °C, a relatively stronger $\sqrt{3}q^*$ can be recognized, implying a HPC structure exclusively formed in the sample. Simultaneously, the diffraction peaks at q = 1.51 $Å^{-1}$ attributed to the crystals of associated THBA emerge in WAXS profiles. A reverse trend can be observed in the heating process of $P4VP_{15k}(THBA)_{0.5}$ as shown in Figure S7 of the Supporting Information. The reason for the formation of lamellar structure around ODT is likely that at higher temperature the hydrogen bonds between THBA and P4VP are weaker, and also the P4VP chains are more coil-like, which thus causes a higher tendency of P4VP to aggregate into layers separated by THBA. As the hydrogen bonding becomes stronger with decreasing temperature, P4VP chains are extended by firmly bonded THBA molecules and turn into cylinder brushlike supramolecules that prefer to pack in a hexagonal manner. Note that the peaks slightly shift to lower q on cooling, possibly due to the more stretched THBA tails at lower temperature. The straightened tails further facilitate the crystallization of the associated THBA below 30 °C. The phase transition of $P4VP_{15k}(THBA)_{0.5}$ with temperature is schematically summarized in Figure S8 of the Supporting Information.

The crystallization behavior between 25 and 40 °C in Figure 8 is rather complicated. In addition to the major crystallization from the associated THBA molecules, it may involve a cocrystallization of the associated THBA with a small amount of free THBA. In the cocrystals, the benzoic acids of free THBA are supposed to form strong intermolecular hydrogen bonding and locate in the middle between supramolecular chains. It has been shown that such an arrangement leads to a nearly doubled d-spacing.[29] The formation of the cocrystals is evidenced by the appearance of a hump at approximately half of the main peak position indicated by the green arrow at 30 °C in SAXS data (Figure 9a). Moreover, the hump disappears upon further cooling, implying the cocrystals reorganize into crystals of associated THBA due to the higher probability to form THBA–P4VP hydrogen bonds at lower temperature. The unusual two adjacent exothermic peaks in DSC curves may thus result from the crystallization and cocrystallization followed by a reorganization in the crystals.

The DSC profiles of $P4VP_{1.7k}(THBA)_x$ at a cooling rate of 1 °C/min are shown in Figure S9 of the Supporting Information. The major difference between $P4VP_{1.7k}(THBA)_x$ and $P4VP_{15k}(THBA)_x$ is that the ODT temperature for $P4VP_{1.7k}(THBA)_x$ is significantly lower, ~36 °C, very close to the crystallization temperature of associated THBA. The *in situ* SAXS and WAXS profiles of $P4VP_{1.7k}(THBA)_{0.5}$ are shown in Figure S10, and the phase transition determined from the scattering data agrees well with the DSC results. Note that the hump at q approximately half of the main peak can be clearly seen in SAXS data at the temperatures where associated THBA crystallizes, indicating the cocrystallization of associated and free THBA also occurs in $P4VP_{1.7k}(THBA)_{0.5}$. The *in situ* SAXS and WAXS profiles of the macrophase-separated samples,

DOI: 10.1021/ma5022192
Macromolecules 2015, 48, 717–724

$P4VP_{1.7k}(THBA)_{0.7}$ and $P4VP_{1.7k}(THBA)_{0.8}$, are shown in Figures S11 and S12, where we can clearly see the diffraction peaks from free THBA crystals below 60 °C.

Polarized optical microscopy (POM) is used to distinguish the ordered structures formed in the cooling process. Figure 10a shows the images at representative temperatures for

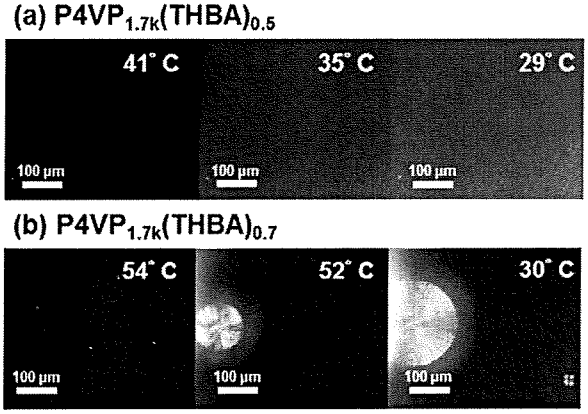

Figure 10. *In situ* POM images of (a) $P4VP_{1.7k}(THBA)_{0.5}$ and (b) $P4VP_{1.7k}(THBA)_{0.7}$ at a cooling rate of 1 °C/min.

$P4VP_{1.7k}(THBA)_{0.5}$ sample. Above ODT temperature, there is no ordered structure so that the image is dark (see the image at 41 °C). At 35 °C, which is slightly below ODT temperature, the locally anisotropic ordered HPC structure exhibits a birefringence and the image turns bluish. At 29 °C, the associated THBA molecules crystallize and the sample becomes more birefringent. For $P4VP_{1.7k}(THBA)_{0.7}$ sample shown in Figure 10b, free THBA form distinct spherulites with strong birefringence at 52 °C. As the temperature reaches 36 °C or lower, the background becomes only slightly bluish due to the formation of limited ordered structure or the crystallization of a very small amount of associated THBA. The complete *in situ* POM images are shown in Figures S13 and S14 of the Supporting Information, and the results are consistent with the DSC curves and scattering data.

4. CONCLUSIONS

We report the degree of complexation, phase behaviors, and structures of a series of supramolecular complexes composed of P4VP hydrogen-bonded with a fanlike benzoic acid derivative with three long hexadecyloxy tails. Because of the high tendency of the small molecule to crystallize, the competition between the self-crystallization of the small molecule and the association of the small molecule onto P4VP results in a maximum degree of complexation, which is different from other systems where the degree of complexation is in general monotonically increased until a saturation is reached. In other words, the crystallization of small molecules induces a dissociation of supramolecules. When the small molecules with such bulky, long tails associate onto polymers, the resulting supramolecular chains are brushlike in shape and tend to organize into hexagonally packed cylinders rather than lamellar structures that are generally formed by comblike supramolecules. The preference for forming cylinder-like chains originates from the steric effect of the long tails. The present study provides an insight into the self-assembly behaviors of supramolecules containing highly crystalline or bulky components, which is useful for efficient preparation and processing of supramolecules.

■ ASSOCIATED CONTENT

Supporting Information

Experimental details for the synthesis and characterization of THBA; schematics of the crystal structure of pure THBA and the phase transition of $P4VP_{15k}(THBA)_{0.5}$ with temperature; supporting FTIR spectra, SAXS and WAXS data, DSC thermograms, and POM images. This material is available free of charge via the Internet at http://pubs.acs.org.

■ AUTHOR INFORMATION

Corresponding Authors

*E-mail shtung@ntu.edu.tw (S.-H.T.).
*E-mail kmlee@nknu.edu.tw (K.-M.L.).

Notes

The authors declare no competing financial interest.

■ ACKNOWLEDGMENTS

This work is financially supported by the grant from the Ministry of Science and Technology, Taiwan (103-2221-E-002-186-MY3). We acknowledge NSRRC, Taiwan, for facilitating the X-ray scattering experiments. We thank Prof. Wen-Bin Liau and Ms. Ya-Hsuan Chen for the assistance in polarized optical microscopy. The assistance in scattering experiments from Dr. Chun-Jen Su, Dr. Yi-Qi Yeh, and Dr. U-Ser Jeng of NSRRC is acknowledged.

■ REFERENCES

(1) Korhonen, J. T.; Verho, T.; Rannou, P.; Ikkala, O. *Macromolecules* **2010**, *43* (3), 1507–1514.
(2) Faber, M.; Hofman, A. H.; Polushkin, E.; van Ekenstein, G. A.; Seitsonen, J.; Ruokolainen, J.; Loos, K.; ten Brinke, G. *Macromolecules* **2013**, *46* (2), 500–517.
(3) Perepichka, I. I.; Borozenko, K.; Badia, A.; Bazuin, C. G. *J. Am. Chem. Soc.* **2011**, *133* (49), 19702–19705.
(4) Chuang, W.-T.; Sheu, H.-S.; Jeng, U. S.; Wu, H.-H.; Hong, P.-D.; Lee, J.-J. *Chem. Mater.* **2009**, *21* (6), 975–978.
(5) Soininen, A. J.; Tanionou, I.; ten Brummelhuis, N.; Schlaad, H.; Hadjichristidis, N.; Ikkala, O.; Raula, J.; Mezzenga, R.; Ruokolainen, J. *Macromolecules* **2012**, *45* (17), 7091–7097.
(6) Rancatore, B. J.; Mauldin, C. E.; Tung, S.-H.; Wang, C.; Hexemer, A.; Strzalka, J.; Fréchet, J. M. J.; Xu, T. *ACS Nano* **2010**, *4* (5), 2721–2729.
(7) Chuang, W.-T.; Lo, T.-Y.; Huang, Y.-C.; Su, C.-J.; Jeng, U. S.; Sheu, H.-S.; Ho, R.-M. *Macromolecules* **2014**, *47* (17), 6047–6054.
(8) Antonietti, M.; Conrad, J.; Thuenemann, A. *Macromolecules* **1994**, *27* (21), 6007–6011.
(9) Zhang, M.; Müller, A. H. E. *J. Polym. Sci., Part A: Polym. Chem.* **2005**, *43* (16), 3461–3481.
(10) Ikkala, O.; Ruokolainen, J.; Torkkeli, M.; Tanner, J.; Serimaa, R.; ten Brinke, G. *Colloids Surf., A* **1999**, *147* (1–2), 241–248.
(11) Ikkala, O.; Ruokolainen, J.; ten Brinke, G.; Torkkeli, M.; Serimaa, R. *Macromolecules* **1995**, *28* (21), 7088–7094.
(12) Ikkala, O.; ten Brinke, G. *Chem. Commun.* **2004**, *19*, 2131–2137.
(13) Ruokolainen, J.; ten Brinke, G.; Ikkala, O. *Adv. Mater.* **1999**, *11* (9), 777–780.
(14) Ikkala, O.; ten Brinke, G. *Science* **2002**, *295* (5564), 2407–2409.
(15) Junnila, S.; Houbenov, N.; Karatzas, A.; Hadjichristidis, N.; Hirao, A.; Iatrou, H.; Ikkala, O. *Macromolecules* **2012**, *45* (6), 2850–2856.
(16) Rancatore, B. J.; Mauldin, C. E.; Fréchet, J. M. J.; Xu, T. *Macromolecules* **2012**, *45* (20), 8292–8299.

DOI: 10.1021/ma5022192
Macromolecules 2015, 48, 717–724

(17) Chen, S. A.; Ni, J. M. *Macromolecules* **1992**, *25* (23), 6081–6089.
(18) Hsu, W. P.; Levon, K.; Ho, K. S.; Myerson, A. S.; Kwei, T. K. *Macromolecules* **1993**, *26* (6), 1318–1323.
(19) Li, C.-L.; Li, M.-C.; Ho, R.-M. *Macromolecules* **2011**, *44* (22), 8898–8907.
(20) Chen, J.-C.; Liu, C.-L.; Sun, Y.-S.; Tung, S.-H.; Chen, W.-C. *Soft Matter* **2012**, *8* (2), 526–535.
(21) Chao, C. Y.; Li, X.; Ober, C. K.; Osuji, C.; Thomas, E. L. *Adv. Funct. Mater.* **2004**, *14* (4), 364–370.
(22) Kosonen, H.; Ruokolainen, J.; Knaapila, M.; Torkkeli, M.; Serimaa, R.; Bras, W.; Monkman, A. P.; ten Brinke, G.; Ikkala, O. *Synth. Met.* **2001**, *121* (1–3), 1277–1278.
(23) Bai, P.; Kim, M. I.; Xu, T. *Macromolecules* **2013**, *46* (14), 5531–5537.
(24) Wu, S.; Bubeck, C. *Macromolecules* **2013**, *46* (9), 3512–3518.
(25) Ruokolainen, J.; Mäkinen, R.; Torkkeli, M.; Mäkelä, T.; Serimaa, R.; ten Brinke, G.; Ikkala, O. *Science* **1998**, *280* (5363), 557–560.
(26) Tung, S.-H.; Kalarickal, N. C.; Mays, J. W.; Xu, T. *Macromolecules* **2008**, *41* (17), 6453–6462.
(27) Huang, W.-H.; Chen, P.-Y.; Tung, S.-H. *Macromolecules* **2012**, *45* (3), 1562–1569.
(28) Wang, S.-J.; Xu, Y.-S.; Yang, S.; Chen, E.-Q. *Macromolecules* **2012**, *45* (21), 8760–8769.
(29) Luyten, M. C.; Alberda van Ekenstein, G. O. R.; ten Brinke, G.; Ruokolainen, J.; Ikkala, O.; Torkkeli, M.; Serimaa, R. *Macromolecules* **1999**, *32* (13), 4404–4410.
(30) Ruokolainen, J.; Torkkeli, M.; Serimaa, R.; Vahvaselkä, S.; Saariaho, M.; ten Brinke, G.; Ikkala, O. *Macromolecules* **1996**, *29* (20), 6621–6628.
(31) Ruokolainen, J.; ten Brinke, G.; Ikkala, O.; Torkkeli, M.; Serimaa, R. *Macromolecules* **1996**, *29* (10), 3409–3415.
(32) Ikkala, O.; Ruokolainen, J.; Torkkeli, M.; Serimaa, R.; ten Brinke, G. *Macromol. Symp.* **1996**, *112* (1), 191–198.
(33) Zhu, X.; Beginn, U.; Möller, M.; Gearba, R. I.; Anokhin, D. V.; Ivanov, D. A. *J. Am. Chem. Soc.* **2006**, *128* (51), 16928–16937.
(34) Liu, X.; Chen, X.; Wang, J.; Chen, G.; Zhang, H. *Macromolecules* **2014**, *47* (12), 3917–3925.
(35) Wang, S.-J.; Zhao, R.-Y.; Yang, S.; Yu, Z.-Q.; Chen, E.-Q. *Chem. Commun.* **2014**, *50* (61), 8378–8381.
(36) Serrette, A. G.; Lai, C. K.; Swager, T. M. *Chem. Mater.* **1994**, *6* (12), 2252–2268.
(37) Jeng, U.-S.; Su, C. H.; Su, C.-J.; Liao, K.-F.; Chuang, W.-T.; Lai, Y.-H.; Chang, J.-W.; Chen, Y.-J.; Huang, Y.-S.; Lee, M.-T.; Yu, K.-L.; Lin, J.-M.; Liu, D.-G.; Chang, C.-F.; Liu, C.-Y.; Chang, C.-H.; Liang, K. S. *J. Appl. Crystallogr.* **2010**, *43* (1), 110–121.
(38) Gao, J.; He, Y.; Liu, F.; Zhang, X.; Wang, Z.; Wang, X. *Chem. Mater.* **2007**, *19* (16), 3877–3881.
(39) Lee, J. Y.; Painter, P. C.; Coleman, M. M. *Macromolecules* **1988**, *21* (4), 954–960.
(40) Takahashi, H.; Mamola, K.; Plyler, E. K. *J. Mol. Spectrosc.* **1966**, *21* (1–4), 217–230.
(41) Reo, R.-J. *Methods of X-ray and Neutron Scattering in Polymer Science*; Oxford University Press: New York, 2000.
(42) Hosono, N.; Kajitani, T.; Fukushima, T.; Ito, K.; Sasaki, S.; Takata, M.; Aida, T. *Science* **2010**, *330* (6005), 808–811.
(43) Ruokolainen, J.; Torkkeli, M.; Serimaa, R.; Komanschek, E.; ten Brinke, G.; Ikkala, O. *Macromolecules* **1997**, *30* (7), 2002–2007.

DOI: 10.1021/ma5022192
Macromolecules 2015, 48, 717–724